

Interfacial Engineering in a Cathode Composite Based on Garnet-Type Solid-State Li-Ion Battery with High Voltage Cycling

Ramkumar Balasubramaniam,^[a] Chan-Woo Nam,^[a] Vanchiappan Aravindan,^[b] Donggun Eum,^[c] Kisuk Kang,^[c] and Yun-Sung Lee^{*[a]}

Garnet-type solid electrolyte is a promising candidate for the fabrication of high energy all-solid-state Li-ion batteries (ASSLIBs), but its use is hampered by a large interfacial resistance. Herein, we propose a surface modification and subsequent sintering to enhance the interfacial connection between the cathode and the solid electrolyte. The ASSLIB prepared by this method delivered an initial discharge capacity of $\sim 66 \text{ mAh g}^{-1}$ (80°C) at a rate of 0.1 C. However, the poor contact between the cathode and electrolyte triggered the increase of the

interfacial resistance, which caused severe capacity decay upon cycling. The encapsulation of LiCoO_2 particles with LiBO_2 using a single-step sintering process dramatically increased the interfacial contact, resulting in a higher discharge capacity of 116 mAh g^{-1} with good cycling behavior. Therefore, surface modification of the cathode offers a reduction of resistance and promotes efficient Li-ion transfer pathways across the cathode/solid-electrolyte interface.

1. Introduction

Over the last three decades, lithium-ion batteries (LIBs) have gained immense attention because of their high energy density, shape versatility, and long-cycle life compared to other rechargeable systems, such as Pb-acid, Ni–Cd, and Ni–MH among others. As a result, Li-ion power packs completely conquered the portable devices and electronic gadget markets, and have also been explored for application in zero-emission transportation and grid storage.^[1] However, the energy density of LIBs is inferior to that of metallic Li because of the utilization of graphitic anodes. In addition, the commercial liquid electrolyte faces issues like cell safety, toxicity, flammability, volatility, formation of dendritic lithium at higher rates, and possible electrolyte leakage.^[2,3] The fabrication of LIBs with solid electrolytes instead of carbonate-based aprotic organic solvents is one of the fascinating approaches to mitigate the aforesaid issues, with the potential to be used at high temperatures ($> 50^\circ\text{C}$).^[4,5] This has a potential impact on zero-emission transportation applications, such as electric vehicles and hybrid electric vehicles.

One of the pre-requisites for the development of Solid-state Li-ion Batteries is a highly ionically conductive solid electrolyte. In addition, a good solid electrolyte requires the following properties: (i) high ionic conductivity at ambient temperature, (ii) low electronic conductivity, (iii) wide electrochemical stability window, (iv) good chemical stability and compatibility with the electrodes, (v) inexpensiveness, and (vi) eco-friendliness.^[1,2,6] Among solid electrolytes, significant preference is given to oxide-based electrolytes, as they offer better compatibility with the electrodes, stability in ambient conditions, and higher reliability than other solid electrolytes (e.g., sulfide-based materials). Generally, oxide-based solid electrolytes are classified based on their crystal structure, namely NASICON $\text{Li}_{1.3}\text{Al}_{0.3}\text{Ti}_{1.7}(\text{PO}_4)_3$ (LATP), perovskite $\text{Li}_{3x}\text{La}_{2/3-x}\text{TiO}_3$ (LLTO), and garnet $\text{Li}_{6.75}\text{La}_3\text{Zr}_{1.75}\text{X}_{0.25}\text{O}_{12}$ (LLZO) type electrolytes.^[7,8] Unfortunately, the titanium reduction (Ti^{4+}) against the Li metal anode eventually enhances the electronic conductivity of the electrolyte material, which limits its potential application as an electrolyte.^[9]

Garnet-type electrolytes are a unique class of materials owing to their super lithophilic nature towards metallic Li; the electrolytes form a surface passivation layer when they come in contact with the metallic substrate.^[9–11] Moreover, Nb-LLZO electrolytes have good chemical and thermal stability, and a wide potential window, which is necessary for high-voltage cathode materials.^[12,13] Generally, garnet-type electrolytes exist in two phases: cubic and tetragonal. The former exhibits maximum ionic conductivity, whereas the later exhibits lower ionic conductivity due to the ordered distribution of Li-ions. To stabilize the cubic phase, structural modification is crucial; thus, iso- and alio-valent doping are employed to improve the ionic conductivity.^[14–17] However, garnet-based electrolytes present a serious high interfacial resistance problem, especially across the electrode-electrolyte interfaces.^[18] Nevertheless, thin-film proc-

[a] R. Balasubramaniam, C.-W. Nam, Prof. Y.-S. Lee
Faculty of Applied Chemical Engineering
Chonnam National University
Gwangju- 500 757, Republic of Korea
E-mail: leey@chonnam.ac.kr

[b] Dr. V. Aravindan
Department of Chemistry
Indian Institute of Science Education and Research (IISER)
Tirupati-517 507, India

[c] D. Eum, Prof. K. Kang
Faculty of Department of Materials Science and Engineering
Seoul National University
Seoul 151-744, Republic of Korea

 Supporting information for this article is available on the WWW under <https://doi.org/10.1002/celc.202001116>

essing using pulsed laser deposition (PLD), aerogel methods, and magnetron sputtering are efficient techniques that can minimize resistance and, subsequently, attain a favorable interfacial contact to fabricate high-performance SSLIBs.^[19–25]

Unfortunately, the previously mentioned thin-film processing techniques are expensive, and they have low energy density due to a small amount of active mass loading. Therefore, these techniques are not suitable for mass production, and an efficient strategy is necessary for the fabrication of high-performance ASSLIBs on a large scale.^[6] In the traditional Li-ion chemistry with liquid electrolyte, the electrodes are formulated with conductive additive and adhesive binders like polyvinylidene fluoride (PVDF). Such a direct slurry coating method is not sufficient to enable a favorable interfacial contact between a cathode and an electrolyte. Engineering the cathode surface is one of the easiest and scalable approaches to overcome the interfacial issues, which is appealing for the mass production of cells. In this regard, a few researchers have recently attempted to use Li_2BO_3 as a sintering additive to enable a favorable interfacial contact during the high-temperature sintering process. However, the specific capacity and cycle life of the ASSLIB were poor because of low capacity utilization, cross-diffusion of elements, and phase transformation.^[6,26–31] In the case of sulfide-based electrolytes, Li_2SiO_3 , LiTaO_3 , $\text{Li}_4\text{Ti}_5\text{O}_{12}$, Li_3PO_4 , and LiNbO_3 were employed as buffer layers to stabilize the interfacial resistance.^[32–38] However, the utilization of the buffer layer is more complicated for oxide-based ceramic electrolytes.^[6,9] Further, several reasons were proposed for the larger charge-transfer/interfacial resistance, e.g., lattice mismatch, space charge layer formation, and inter-diffusion of elements.^[39,40,41,32] Therefore, interfacial engineering is strongly recommended as an effective strategy to dilute the charge-transfer resistance during the fabrication of the ASSLIB.^[42,45–49]

In the present work, we investigated the use of LiBO_2 as a sintering aid to formulate the composite LiCoO_2 cathode, to facilitate the interfacial contact between the cathode and the electrolyte in the ASSLIB. $\text{Li}_{6.75}\text{La}_3\text{Zr}_{1.75}\text{Nb}_{0.25}\text{O}_{12}$ was used as a solid-state electrolyte, and Li metal served as a counter electrode. The ball milling procedure was used to encapsulate the LiCoO_2 particles with LiBO_2 . The LiBO_2 modification in the LCO particles not only enhance the ionic conductivity of the cathode composite, but also improving the mechanical property of the SSB. It should be noted that the LiBO_2 layer between the cathode particles will improve its contact during sintering, which will help ensure the interconnectivity between cathode particles that determines the electronic conductivity of the electrode. It is worth mentioning that the ASSLIB was tested in a wider potential window than the routine window of 4.3 V vs. Li. As expected, the LiBO_2 modified LiCoO_2 -based ASSLIB exhibited improved interfacial contact, which resulted in better electrochemical performance and cycle life. Our aim was to develop an ASSLIB for high-temperature operation; therefore, the electrochemical studies were conducted only at a temperature of 80 °C.

Experimental Section

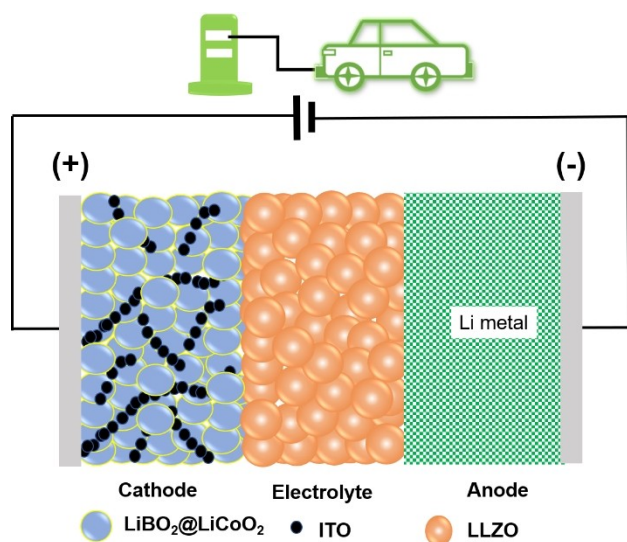
A traditional solid-state route was adopted to prepare the $\text{Li}_{6.75}\text{La}_3\text{Zr}_{1.75}\text{Nb}_{0.25}\text{O}_{12}$ electrolyte.^[17] Briefly, $\text{LiOH}\cdot\text{H}_2\text{O}$, La_2O_3 , ZrO_2 , and Nb_2O_5 precursors were ball milled for 24 h in ethanol solution with 10% excess of $\text{LiOH}\cdot\text{H}_2\text{O}$. After solvent evaporation, the powder was calcined at 950 °C for 18 h in air. Then, the calcined powder was wet ball milled for 24 h and dried. Finally, the garnet powder was pressed into a pellet and subsequently sintered at 1050 °C for 12 h in an O_2 atmosphere, covered by the mother powder (calcined powder at 950 °C) to suppress the loss of lithium. After the sintering process, the pellet was employed as a solid electrolyte for further electrochemical studies. In this study, commercial LiCoO_2 powder was used as the cathode material.

Physical characterization

Powder X-ray diffraction (XRD; Cu $\text{K}\alpha$ radiation, Rint 1000, Rigaku, Japan) was performed to analyze the crystal structures of the synthesized phase. Field emission scanning electron microscopy (FE-SEM; S-4700, Hitachi, Japan) and high-resolution transmission electron microscopy (HR-TEM; JEM-2000, EX-II, JEOL, Japan) coupled with energy-dispersive X-ray spectroscopy (EDX) were used to analyze the particle surface morphology, cross-sectional interface, and elemental composition of the material.

Electrochemical Characterization

The A.C. (alternating current) impedance study was performed to measure the ionic conductivity using a 4284 A Precision LCR Meter between 1 MHz and 20 mHz with an applied voltage of 10 mV. The electronic conductivities of Nb-LLZO at different temperatures were measured by applying a 0.1 V DC voltage on the Pt/Nb-LLZO/Pt cell. Prior to the impedance measurement, the LLZO pellet (10 mm diameter, 0.1 mm thickness) was prepared, and Pt was coated on both sides. The ASSLIB was assembled using Nb-LLZO as the electrolyte, LCO composite (LiCoO_2) as the cathode, and Li metal as the anode. The LiCoO_2 surface was homogeneously covered with LiBO_2 (Strem co. Ltd) by ball milling. The ratio of LiCoO_2 to LiBO_2 was fixed at 90:10 weight ratio, and the LiBO_2 -coated LiCoO_2 was ball milled at 100 rpm for 1 h. For the formulation of the composite cathode, LiCoO_2 , with or without the LiBO_2 coating, and indium tin oxide (ITO) were mixed in a weight ratio of 85:10:5 and additionally mixed with an ethyl cellulose binder. The binder molecules functional groups absorb onto the cathode particle surface by chemical bonding, so the conductive network formed in the cathode composite. Subsequently, it was mixed with *N*-Methyl-2-pyrrolidone (NMP) to prepare the cathode slurry. The slurry was drop-casted on the surface of the Nb-LLZO pellet (thickness of the pellet = 1 cm), and the solvent was removed by drying inside an Ar-filled glove box. The casted pellet was subjected to heat treatment at 700 °C for 1 h (Oxygen atmosphere) to enable better contact. Li metal foil was attached to the other side of the pellet by heating at 200 °C for 30 min. All the electrochemical studies were performed using a 2032 coin-cell at 80 °C. (Scheme 1) A Bio-logic (SP-150, France) electrochemical workstation was used to analyze the cyclic voltammetry (CV) and the electrochemical impedance spectroscopy. A Won-A-Tech battery tester (WBCS 3000, Korea) was used to study the charge-discharge performance of the battery between 3–4.5 V vs. Li at 0.1 C rate ($14\text{ }\mu\text{A cm}^{-2}$). For further comparison, we prepared a liquid cell consisting of LiCoO_2 as the cathode and Li metal as the anode, separated by a polypropylene separator with 1 M LiPF_6 in ethylene carbonate: dimethyl carbonate (with 1:1 v/v ratio) as the electrolyte. The electrochemical performance of the liquid cell was tested at 25 °C.



Scheme 1. Typical schematic diagram for all-solid-state Li-ion batteries (ASSLIBs).

2. Results and Discussion

The Figure 1 illustrates the Rietveld refinement XRD pattern of the LCO + Nb-LLZO after sintering at 700 °C for 1 h. The diffraction pattern of the interface well-matched with LiCoO₂ and Nb-LLZO. This indicates that no impurity formation between the LCO composite and the Nb-LLZO electrolyte interface under this sintering condition. The obtained lattice and other refined parameters have been summarized in Table S1.

Figure S1a shows the XRD pattern of the synthesized Nb-LLZO solid electrolyte. The obtained pattern shows well-defined reflections corresponding to the cubic phase with the space group of Ia-3d.^[17] Further, it is observed that the XRD pattern exhibits no additional peaks corresponding to the impurity phases. The calculated lattice parameter value reveals the formation of a cubic structure with a lattice constant of 12.99 Å. Figure S1b shows well-defined XRD peaks representing the

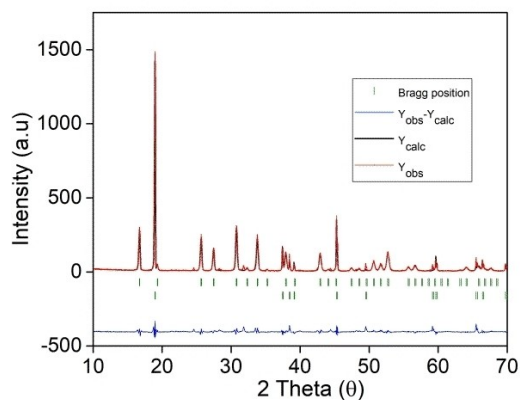


Figure 1. The Rietveld refinement XRD result for LiCoO₂ + Nb-LLZO at 700 °C for 1 hour ($R_p = 11.5\%$).

hexagonal structure with the R-3m space group of the commercial LiCoO₂ particles. The ionic conductivity of the prepared Nb-LLZO solid electrolyte was calculated as $1.74 \times 10^{-5} \text{ S cm}^{-1}$ and $2.72 \times 10^{-4} \text{ S cm}^{-1}$ at 25 °C and 80 °C, respectively (Figure S1c). The ionic conductivity of the solid electrolyte is slightly inferior ($\sim 1 \times 10^{-4} \text{ S cm}^{-1}$) compared to the literature, which is mainly due to the low relative density of 74%. The electronic conductivity of the prepared solid electrolyte was $1 \times 10^{-8} \text{ S cm}^{-1}$ and $1.74 \times 10^{-6} \text{ S cm}^{-1}$ at 25 °C and 80 °C. (Figure S1d) The average particle size of the Nb-LLZO powder is in the range of 1–5 μm, which is evident from the FE-SEM images (Figure S2). The elemental distribution map obtained from the electrolyte powder revealed that La³⁺, Zr⁴⁺, and Nb⁵⁺ were homogeneously distributed throughout the electrolyte.

Figure S6 shows the FE-SEM picture of the surface morphology of the LiCoO₂ particles. It is obvious that the primary LiCoO₂ particle size is in the range of 1–5 μm. Furthermore, an attempt was made to employ LiBO₂ for modifying the LiCoO₂ surface, which is anticipated to alter the interface between electrode and electrolyte. Figure 2 shows the TEM images of the surface modified LiCoO₂ powder. The LiBO₂ is covering the surface of the LiCoO₂ particles, which is clear from the elemental distribution of the particles (Figure 3). Figure 2c–e illustrates the HR-TEM picture of the LiCoO₂ cathode after LiBO₂ modification. We additionally provided the FESEM-EDS mapping and XPS results for LiBO₂ was coated on the surface of LCO particles. [Figure S3–S5] Obviously, a layer has effectively covered the surface of the LiCoO₂ particles, which is associated to each other, corresponding to the LiBO₂ modification. The surface modification increases the active region of the LiCoO₂ particles and is expected to enhance the electrochemical performance of the SSLIBs. Noticeably, at high temperatures (700 °C), the LiBO₂

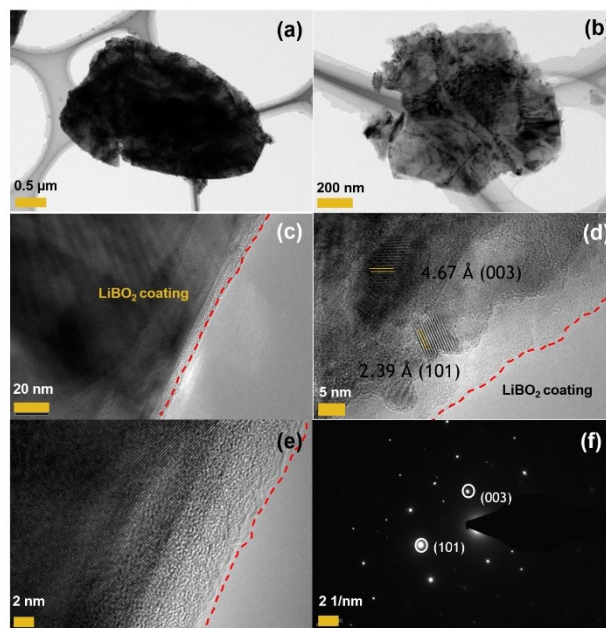


Figure 2. TEM images of LiBO₂ coated LiCoO₂ particles. a, b, c) TEM images, d, e) HR-TEM images, and f) SAED pattern of the LiBO₂ coated LiCoO₂ particles.

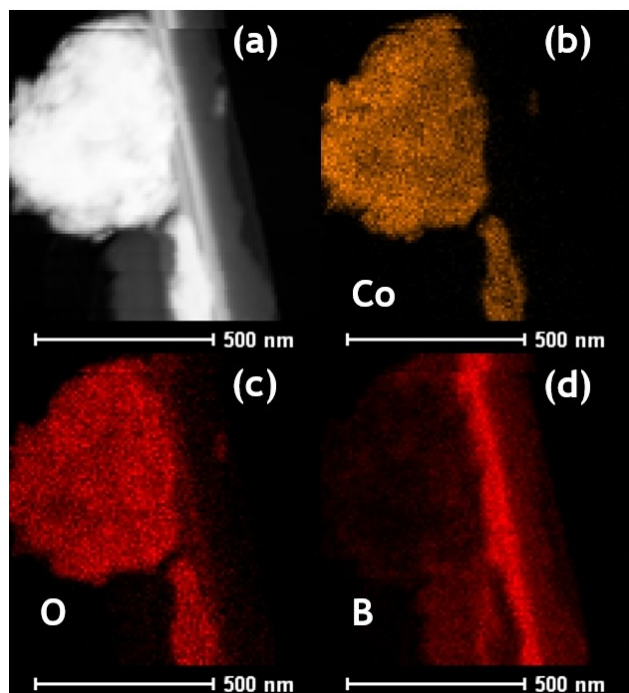


Figure 3. Elemental distribution mapping image of LiBO_2 coated LiCoO_2 particles. a) LiBO_2 - LiCoO_2 particle, b) cobalt, c) oxygen, and d) boron elemental mapping images.

liquid phase occupy the void between the LiCoO_2 particles upon the fabrication of the cell.^[30]

The cross-sectional image of the interface between the LiCoO_2 composite and the Nb-LLZO garnet solid electrolyte is shown in Figures 4a and b. As mentioned earlier, the composite cathode contains bare- LiCoO_2 or LiBO_2 coated LiCoO_2 , ITO, and ethyl cellulose binder fabricated by slurry casting and subsequent sintering at 700°C . The cathode composite thickness was approximately $10\text{--}15\ \mu\text{m}$. Figure 4a revealed the inefficient interfacial contact between the bare LiCoO_2 composite and the Nb-LLZO electrolyte due to poor wettability of the cathode

materials. In the case of the LiBO_2 coated LiCoO_2 cell sintered at 700°C , the LiBO_2 liquid phase filled the spaces/voids between the LiCoO_2 particles and the Nb-LLZO solid electrolyte.^[26] The cross-sectional image further confirmed that the cathode composite and the solid electrolyte have a favorable interfacial contact between them (Figure 4b). The elemental line map shows a clear difference between the LiCoO_2 composite cathode and the Nb-LLZO solid electrolyte. Figure S7 revealed the clear distribution of Co and La in the interface between the LCO composite and the Nb-LLZO electrolyte. Only a trace number of ions migrated because of high-temperature treatment. Finally, it is worth mentioning the inevitable side reaction between the cathode composite and the electrolyte at high temperature with Co and La crossover.^[28]

To utilize the full capacity of the LiCoO_2 cathode, the cell was tested at high voltage regime up to $4.5\ \text{V}$ vs. Li. Figure 5a illustrates the galvanostatic charge/discharge curve for the ASSLIB up to 5 cycles at 80°C and a current rate of $0.1\ \text{C}$ ($14\ \mu\text{A}\ \text{cm}^{-2}$). The ASSLIB delivered the capacity of approximately 107 and $66\ \text{mAhg}^{-1}$, for 1st charge and discharge, respectively. Apparently, the capacity decay is due to a lack of physical contact in the solid-solid interface and the irreversible electrochemical reaction in the first charge-discharge process.^[28] In Figure 5b, the dQ/dV vs. potential curve of the ASSLIB revealed the narrow oxidation and wide reduction peak upon the charge and discharge process. The slow reaction kinetics across the contact between the cathode particles and the Nb-LLZO electrolyte system is the main reason for this observation. After 25 cycles, the SSLIB retained the discharge capacity of only $\sim 19\ \text{mAhg}^{-1}$ with a retention of 29% (Figure 5c). As expected, the ASSLIB rendered the coulombic efficiency of $\sim 62\%$ in the first cycle. Nevertheless, the coulombic efficiency reached $>99\%$ after the 3rd cycle. Afterwards, the charge and discharge capacity remained roughly constant, which indicates the stable interface formed in the ASSLIB (Figure 5c).^[43,44] The prime reason for the capacity decay in the ASSLIB was the formation of the highly-resistive/robust space charge layer across the cathode/electrolyte interface.^[33] Generally, in a battery, the charge-

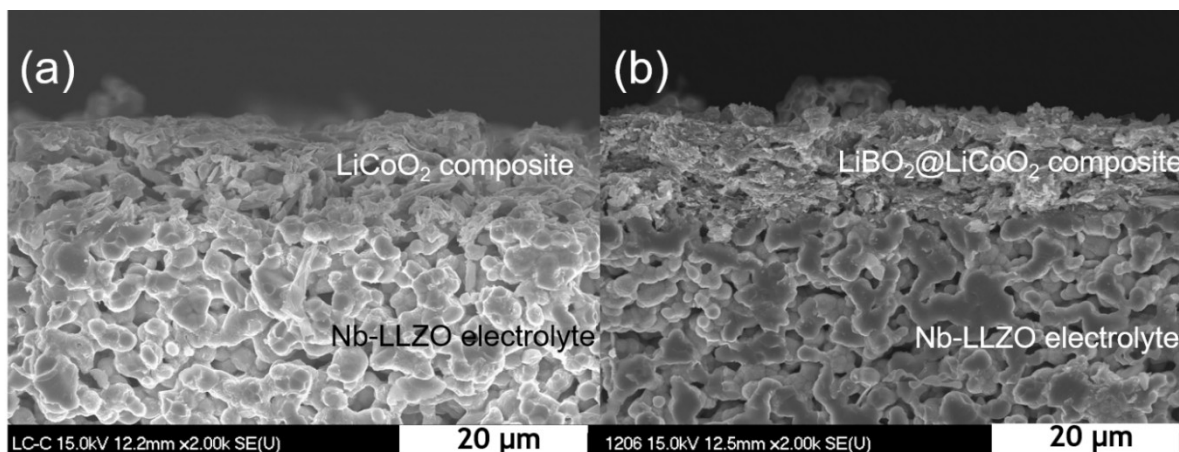


Figure 4. Cross-sectional image of the LiCoO_2 composite and Nb-LLZO interface. a) Bare LiCoO_2 /Nb-LLZO interface, b) LiBO_2 coated LiCoO_2 composite and Nb-LLZO interface.

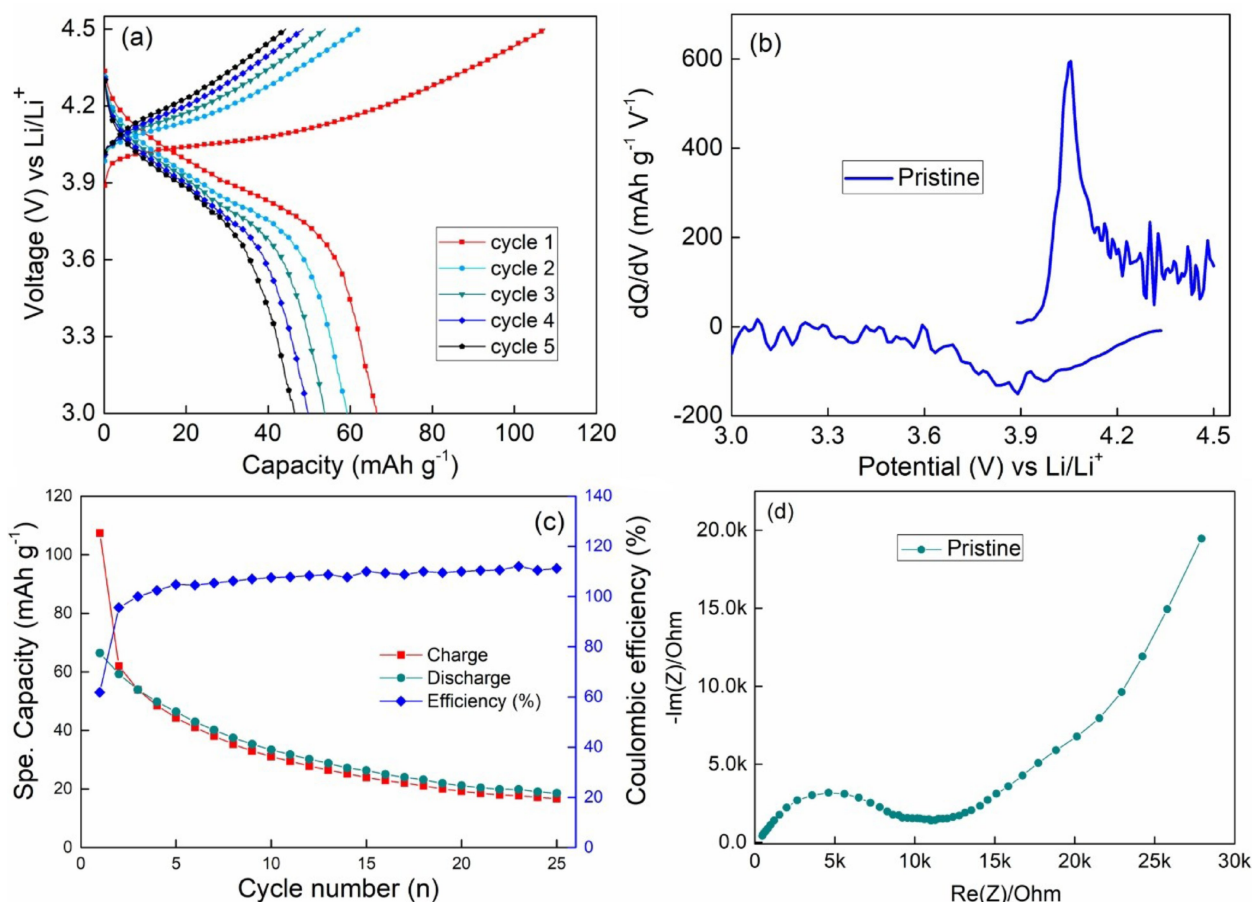


Figure 5. Electrochemical performance of pristine LiCoO₂-based ASSLIBs tested at 80 °C. a) Typical galvanostatic charge-discharge curves at 0.1 C, b) differential capacity profile, c) cycling profile with coulombic efficiency, and d) EIS curve.

transfer resistance, R_{ct} , is affected by the interfacial charge distribution, which is important for the electrochemical performance. For charging, the Li-ions are transferred from the cathode to the electrolyte, and a Li depletion layer is formed in the interface, which is attributed to the potential difference between the cathode and the electrolyte causing a large deviation in R_{ct} .^[6,41] The value of R_{ct} derived from the curve (Figure 5d) is found to be 10.6 kΩ for the pristine LCO based ASSLIB. The obtained R_{ct} value was higher in the pristine cathode because of the large polarization at the interface, which eventually leads to a severe capacity decay. To mitigate the aforesaid shortcomings, a suitable interface modification is necessary to reduce the interfacial resistance between the cathode and electrolyte.^[36,38] For comparison, we added the liquid cell results to the supporting information (Figure S8). The cells provide good electrochemical performance, which indicates the facile Li-ion transfer pathway in the pristine LiCoO₂ composite because of the liquid-solid interface.

The electrochemical performance of LiBO₂-coated LiCoO₂ in SSLIB was evaluated at 80 °C and given in Figure 6. Figures 6a and 6c represent the typical galvanostatic charge-discharge curve and coulombic efficiency profile of ASSLIB fabricated using the surface-treated LiCoO₂ powder. The surface-treated LiCoO₂ powder exhibited a high initial discharge capacity of

116 mAh g⁻¹, and the capacity remained as high as 64 mAh g⁻¹ after the 25th cycle with a corresponding capacity retention of 55%. Noticeably, the surface treatment has enhanced the cycling performance of the battery. In Figure 6b, the dQ/dV vs. potential (V) curve of the ASSLIB shows the prominent oxidation and reduction peaks for the Li intercalation and deintercalation of Li-ions from the LiCoO₂ cathode.^[2,29] The surface-treated LCO-based SSLIB displayed reduced polarization compared with its pristine configuration. Rate Capability is a key factor for large-scale application of LIB. Hence, the rate capability of the ASSLIBs was studied in a voltage range of 3–4.5 V at current densities of 0.05 C to 0.2 C rate as plotted in Figure S9. The bare LCO displayed specific capacities of 103, 54 and 26 mAh g⁻¹ at current densities of 0.05, 0.1 and 0.2 C respectively, whereas LiBO₂ coated LCO showed enhanced capacities of 140, 100 and 48 mAh g⁻¹, respectively. The surface modification of the cathode particles effectively connecting the active material at high temperature helps to decrease the cell polarization and increase the discharge capacity.^[6,36,38] The impedance spectra (Figure 6d) was used to calculate R_{ct} . A semicircle in the medium frequency region is ascribed to the charge-transfer resistance across the electrode/electrolyte interface. The value of R_{ct} resulting from the curve was 3.1 kΩ for the cell with LiBO₂-coated LiCoO₂ particles, which was much lower than that of the

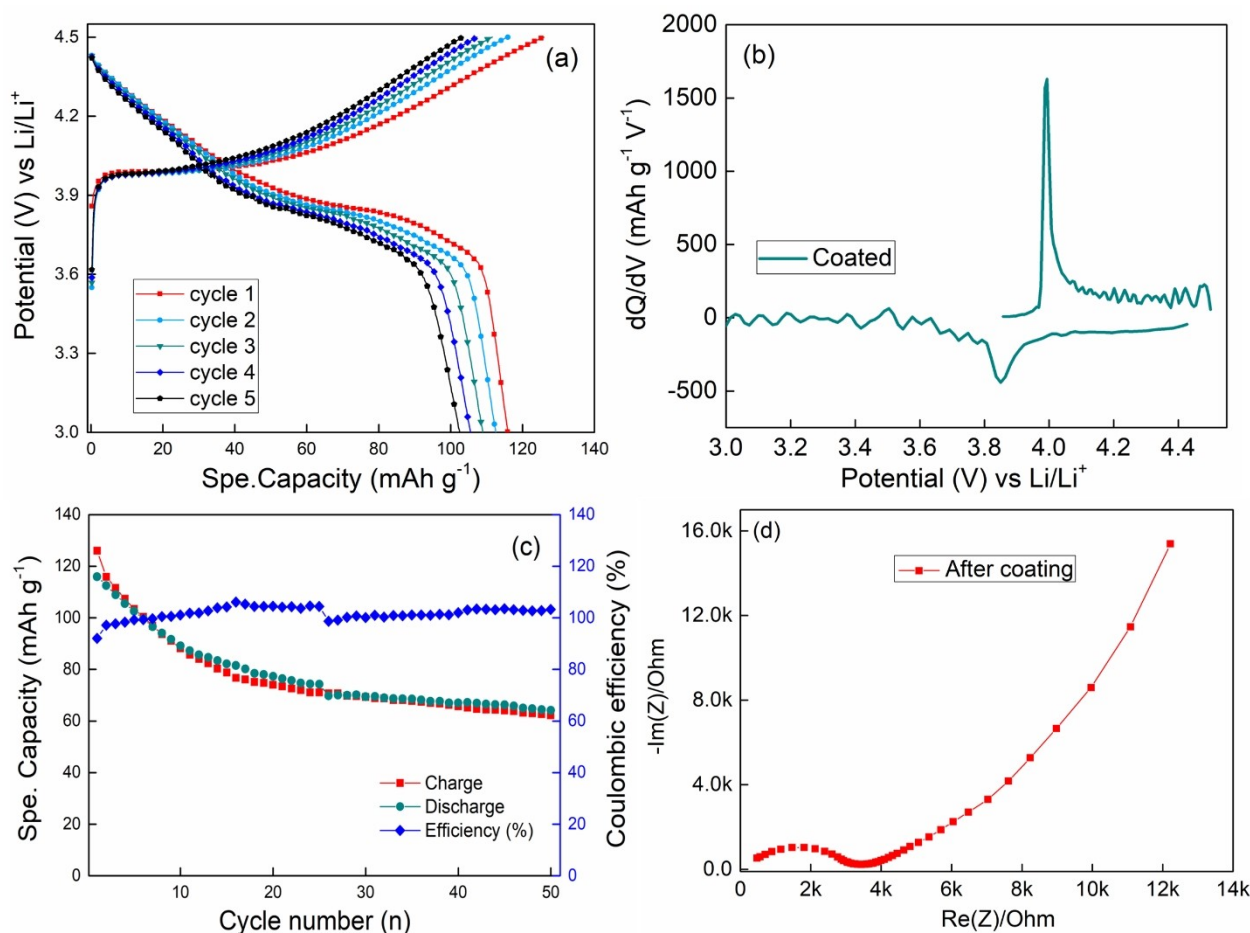


Figure 6. Electrochemical performance of the LiBO_2 -coated LiCoO_2 composite based ASSLIB at 80°C . a) Galvanostatic charge-discharge curve for the first 5 cycles at 0.1 C rate, b) differential capacity profile, c) cycling stability curve along with coulombic efficiency curve, and d) electrochemical impedance curve, of the LiBO_2 -coated LCO composite in SSLIBs.

pristine LiCoO_2 composite. Apparently, the dilution of R_{ct} value can be attributed to the surface modification of the active material, thus leading to lower polarization in the interface region.^[6,38] Hence, the surface modification of LiCoO_2 through LiBO_2 coating demonstrated to be an operative process to enhance the electrochemical performance of ASSLIB in facets of high reversible capacity and retention.

Our results were compared with previously reported Nb-LLZO-based solid-state battery systems, as shown in Table S2. The results demonstrated that our interface engineered cathode composite system provided higher capacity than other reported works. The reason for the capacity degradation in the electrochemical process was mainly associated with the mechanical degradation of the interface due to the large volume change in the LiCoO_2 electrode particles (Figure S10 and S11).^[31] We anticipate the improvement of the mechanical strength and cycle life of the battery by mixing electrolyte with the cathode composite material.^[29]

3. Conclusions

An all-solid-state Li-ion battery was successfully fabricated with a Nb-LLZO electrolyte, LiCoO_2 composite cathode, and Li metal anode. The interfacial contact between the cathode active material was increased by LiBO_2 modification. The modified cathode in the ASSLIB rendered a high initial discharge capacity of 116 mAh g^{-1} with 64% retention after 25 cycles at 80°C . The LiBO_2 coating of the LiCoO_2 powders decreased R_{ct} , which decreased the cell polarization, therefore providing enhanced reversibility, capacity retention, and coulombic efficiency. Further in-depth studies and optimization are necessary to improve the capacity retention characteristics and to enable operation at room temperature.

Acknowledgments

The authors gratefully acknowledge the financial support from the Ministry of Trade, Industry & Energy, Republic of Korea (10080314). VA thank the financial support from the Science & Engineering Research Board (SERB), a statutory body of the Department of

Science & Technology, Govt. of India, through Ramanujan Fellowship (SB/S2/RJN-088/2016).

Conflict of Interest

The authors declare no conflict of interest.

Keywords: all-solid-state lithium battery • high-voltage cathode • solid electrolyte • induced cracks • interfacial resistance

- [1] V. Thangadurai, S. Narayanan, D. Pinzar, *Chem. Soc. Rev.* **2014**, *43*, 4714–4727.
- [2] R. Chen, W. Qu, X. Guo, L. Li, F. Wu, *Mater. Horiz.* **2016**, *3*, 487–516.
- [3] Y. Wang, W. D. Richards, S. P. Ong, J. L. Miara, J. C. Kim, Y. Mo, G. Ceder, *Nat. Mater.* **2015**, *14*, 1026–1032.
- [4] B. Zhang, R. Tan, L. Yang, J. Zheng, K. Zheng, S. Mo, Z. Lin, F. Pan, *Energy Storage Mater.* **2018**, *10*, 139–159.
- [5] B. Wu, S. Wang, W. J. Evans, D. Z. Deng, J. Yang, J. Xiao, *J. Mater. Chem. A* **2016**, *4*, 15266–15280.
- [6] T. Liu, Y. Zhang, X. Zhang, L. Wang, S. Zhao, Y. Lin, Y. Shen, J. Luo, L. Li, C. W. Nan, *J. Mater. Chem. A* **2018**, *6*, 4649–4657.
- [7] Z. Zhang, Y. Shao, B. Lotsch, Y. S. Hu, H. Li, J. Janek, L. F. Nazar, C. W. Nan, J. Maier, M. Armand, L. Chen, *Energy Environ. Sci.* **2018**, *11*, 1945–1976.
- [8] Y. Ren, K. Chen, R. Chen, T. Liu, Y. Zhang, C. W. Nan, *J. Am. Ceram. Soc.* **2015**, *98*, 3603–3623.
- [9] K. Fu, Y. Gong, B. Liu, Y. Zhu, S. Xu, Y. Yao, W. Luo, C. Wang, S. D. Lacey, J. Dai, Y. Chen, Y. Mo, E. Wachsman, L. Hu, *Sci. Adv.* **2017**, *3*, 1601659.
- [10] W. Luo, Y. Gong, Y. Zhu, K. K. Fu, J. Dai, S. D. Lacey, C. Wang, B. Li, X. Han, Y. Mo, E. D. Wachsman, L. Hu, *J. Am. Chem. Soc.* **2016**, *138*, 12258–12262.
- [11] Y. Li, X. Chen, A. Dolocan, Z. Cui, S. Xin, L. Xue, H. Xu, K. Park, J. B. Goodenough, *J. Am. Chem. Soc.* **2018**, *140*, 6448–6455.
- [12] Y. Ren, T. Liu, Y. Shen, Y. Lin, C. W. Nan, *J. Mater.* **2016**, *2*, 256–264.
- [13] T. Thompson, S. Yu, L. Williams, R. D. Schmidt, R. Garcia-Mendez, J. Wolfenstine, J. L. Allen, E. Kioupakis, D. J. Siegel, J. Sakamoto, *ACS Energy Lett.* **2017**, *2*, 462–468.
- [14] R. Murugan, V. Thangadurai, W. Weppner, *Angew. Chem. Int. Ed.* **2007**, *46*, 7778–7781.
- [15] Y. Ren, H. Deng, R. Chen, Y. Shen, Y. Lin, C. W. Nan, *J. Eur. Ceram. Soc.* **2015**, *35*, 561–572.
- [16] T. Thompson, A. Sharafi, M. D. Johannes, A. A. Huq, J. L. Allen, J. Wolfenstine, J. Sakamoto, *Adv. Energy Mater.* **2015**, *5*, 1500096.
- [17] W. Gu, M. Ezbir, R. P. Rao, M. Avdeev, S. Adams, *Solid State Ionics* **2015**, *274*, 100–105.
- [18] C. Sun, J. Liu, Y. Gong, D. P. Wilkinson, J. Zhang, *Nano Energy* **2017**, *3*, 363–386.
- [19] T. Kato, T. Hamanaka, K. Yamamoto, T. Hirayama, F. Sagane, Motoyama, Y. Iriyama, *J. Power Sources* **2014**, *260*, 292–298.
- [20] K. H. Kim, Y. Iriyama, K. Yamamoto, S. Kumazaki, T. Asaka, K. Tanabe, C. A. J. Fisher, T. Hirayama, R. Murugan, Z. Ogumi, *J. Power Sources* **2011**, *196*, 764–767.
- [21] S. Ohta, T. Kobayashi, J. Seki, T. Asaoka, *J. Power Sources* **2012**, *202*, 332–335.
- [22] C. W. Ahn, J. J. Choi, J. Ryu, B. D. Hahn, J. W. Kim, W. H. Yoon, J. H. Choi, D. S. Park, *J. Electrochem. Soc.* **2015**, *162*, A60–A63.
- [23] R. Inada, K. Okuno, S. Kito, T. Tojo, Y. Sakurai, *Materials* **2018**, *11*, 1570.
- [24] G. Vardar, W. J. Bowman, Q. Lu, J. Wang, R. J. Chater, A. Aguiadero, R. Seibert, J. Terry, A. Hunt, I. Waluyo, D. D. Fong, A. Jarry, E. J. Crumlin, S. L. Hellstrom, Y. M. Chiang, B. Yildiz, *Chem. Mater.* **2018**, *30*, 6259–6276.
- [25] M. Kotobuki, K. Kanamura, Y. Sato, T. Yoshida, *J. Power Sources* **2011**, *196*, 7750–7754.
- [26] S. Ohta, S. Komagata, J. Seki, T. Saeki, S. Morishita, T. Asaoka, *J. Power Sources* **2013**, *238*, 53–56.
- [27] S. Ohta, J. Seki, Y. Yagi, Y. Kihira, T. Tani, T. Asaoka, *J. Power Sources* **2014**, *265*, 40–44.
- [28] K. Park, B. C. Yu, J. W. Jung, Y. Li, W. Zhou, H. Gao, S. Son, J. B. Goodenough, *Chem. Mater.* **2016**, *28*, 8051–8059.
- [29] T. Liu, Y. Ren, Y. Shen, S. X. Zhao, Y. Lin, C. W. Nan, *J. Power Sources* **2016**, *324*, 349–357.
- [30] T. Liu, Y. Zhang, R. Chen, S. X. Zhao, Y. Lin, C. W. Nan, Y. Shen, *Electrochem. Commun.* **2017**, *79*, 1–4.
- [31] F. Han, J. Yue, C. Chen, N. Zhao, Z. Fan, Z. Ma, T. Gao, F. Wang, X. Guo, C. Wang, *Joule* **2018**, *2*, 497–508.
- [32] A. Sakuda, A. Hayashi, M. Tatsumisago, *Chem. Mater.* **2010**, *22*, 949–956.
- [33] K. Takada, N. Ohta, L. Zhang, K. Fukuda, I. Sakaguchi, R. Ma, M. Osada, T. Sasaki, *Solid State Ionics* **2008**, *179*, 1333–1337.
- [34] K. Takada, *Langmuir* **2013**, *29*, 7538–7541.
- [35] Y. Ito, Y. Sakurai, S. Yubuchi, A. Sakuda, A. Hayashi, M. Tatsumisago, *J. Electrochem. Soc.* **2015**, *162*, A1610–A1616.
- [36] K. Takada, N. Ohta, L. Zhang, X. Xu, B. T. Hang, T. Ohnishi, M. Osada, T. Sasaki, *Solid State Ionics* **2012**, *225*, 594–597.
- [37] T. Ohtomo, A. Hayashi, M. Tatsumisago, Y. Tsuchida, S. Hama, K. Kawamoto, *J. Power Sources* **2013**, *233*, 231–235.
- [38] N. Ohta, K. Takada, I. Sakaguchi, L. Zhang, R. Ma, K. Fukuda, M. Osada, T. Sasaki, *Electrochem. Commun.* **2007**, *9*, 1486–1490.
- [39] J. Maier, *Phys. Chem. Chem. Phys.* **2009**, *11*, 3011–3022.
- [40] J. Maier, *Prog. Solid State Chem.* **1995**, *23*, 171–263.
- [41] J. Haruyama, K. Sodeyama, L. Han, K. Takada, Y. Tateyama, *Chem. Mater.* **2014**, *26*, 4248–4255.
- [42] J. V. D. Broek, S. Afyon, J. L. M. Rupp, *Adv. Energy Mater.* **2016**, *6*, 1–11.
- [43] C. L. Tsai, Q. Ma, C. Dellen, S. Lobe, F. Vondahlen, A. Windmüller, D. Grüner, H. Z. Heng, S. Uhlenbruck, M. Finsterbusch, F. Tietz, D. Fattakhova-Rohlfing, H. P. Buchkremer, O. Guillon, *Sustain. Energy Fuels* **2019**, *3*, 280–91.
- [44] K. Nie, Y. Hong, J. Qiu, Q. Li, X. Yu, H. Li, L. Chen, *Front. Chem.* **2018**, *6*, 1–19.
- [45] F. Han, J. Yue, C. Chen, N. Zhao, X. Fan, Z. Ma, T. Gao, F. Wang X Guo, C. Wang, **2018**, *2*, 497–508.
- [46] N. Zhao, W. Khokhar, Z. Bi, C. Shi, X. Guo, L. Z. Fan, C. W. Nan, **2019**, *3*, 1190–1199.
- [47] B. Sun, Y. Jin, J. Lang, K. Li, M. Fang, H. Wu, *Chem. Commun.* **2019**, *55*, 6704–6707.
- [48] T. Zhang, W. He, W. Zhang, T. Wang, P. Li, Z. Sun, X. Yu, *Chem. Sci.* **2020**, *11*, 8686–8707.
- [49] X. B. Cheng, C. Z. Zhao, Y. X. Yao, H. Liu, Q. Zhang, **2019**, *5*, 74–96.

Manuscript received: August 25, 2020

Revised manuscript received: October 30, 2020

Accepted manuscript online: November 16, 2020